Modeling a Detection of Internally Reflected Cherenkov Light (DIRC) Particle Detector for High-Multiplicity Collisions

Wilka Carvalho*
Stony Brook University
(Dated: August 17, 2015)

This paper aims to explore the feasibility of using a Detection of Internally Reflected Cherenkov light (DIRC) to identify particles in high-multiplicity events. In order to study this question, we are developing a particle identification (PID) algorithm that identifies particles from high-multiplicity collisions that intersect with a DIRC. We model the DIRC and use a Monte Carlo to generate the Cherenkov light data one would obtain from it. The PID algorithm operates on this data. It consists of a pattern recognition algorithm that correlates the angular distribution of the Cherenkov light to the trajectories of each particle that produced it. We attempt to reduce the analyses of high-multiplicity events into analyses of low- to single-multiplicity events. By doing so, we extend the DIRC's proven efficacy in low-multiplicity events to high-multiplicity events.

INTRODUCTION

We are interested in studying whether a Detection of Internally Reflected Cherenkov light (DIRC) particle detector can be used to identify particles from high-multiplicity collisions. This paper will first motivate the choice to use a DIRC, citing relevant previous success. We will follow with an overview of relevant DIRC concepts and functionality. Next, we will discuss specifications for the DIRC we modeled, the Monte Carlo used to generate Cherenkov light data, and the PID algorithm we have developed to test the DIRC at high-multiplicity. The PID algorithm will be this paper's main topic of discussion as it details the DIRC's performance at various levels of multiplicity, most notably high-multiplicity. We will conclude with a summary of our PID algorithm's performance.

Physics Motivation

It is common for colliders such as the Relativistic Heavy Ion Collider to run experiments that produce events of high-multiplicity. In these experiments, details of the particle production in the collision are largely unknown. Understanding these details may bring insight into the forces (such as the strong force) driving particle production in these events.

Particle detectors are employed to learn about these details. They generally consist of 3 components: tracking detectors, PID detectors, and caloriometers. Tracking detectors in conjuction with a magnetic field are used to determine the momentum of particles, PID detectors determine the velocity of particles, and calorimeters determine the energy of particles. In this study, we focus on the second component, a PID detector - our solution is a DIRC detector. We assume that there is a tracking system that provides momentum, and position information at the location of the DIRC.

DIRC overview

A Detection of Internally Reflected Cherenkov light (DIRC) particle detector is a ring-imaging Cherenkov counter (RICH) [1]. RICH's function by utilizing Cherenkov light. DIRCs, specifically, consists of a radiator (such as quartz) and a light-sensitive detector at the end. The radiator both preserves angular information and guides the Cherenkov light to the detector surface. There, the light's angular information is recorded [2]. Typically, the radiator has a simple form (a rectangular bar in our case) in order to minimize the complexity of the resultant angular distribution of the light due to reflections inside the radiator.

When a charged particle traverses through a radiator medium with index of reflection $n > 1$, it emits Cherenkov light (photons) at a well defined angle θ_e given by

$$\theta_e = cos^{-1}\left(\frac{1}{n\beta}\right) \tag{1}$$

where $\beta = v_P/c$, v_P is the speed of the particle and c is the speed of light. β is related to the particle's mass m and momentum p via

$$\beta = \frac{p}{(m^2 v_P^2 + p^2)^{1/2}}. \tag{2}$$

Photons are maintained within the radiator by total internal reflection. The critical angle above which photons are reflected within the radiator is given by

$$|\Theta_e| > \Theta_c = sin^{-1}\left(\frac{1}{n}\right), \tag{3}$$

where Θ_e is a solid angle described by (θ_e, ϕ_e) as in Figure (1) (ϕ_e is an arbitrary angle between 0 and 2π). Photons maintained due to total internal reflection can be analyzed along with knowledge of a particle's trajectory and momentum to determine its identity. One can find a visual representation of a particle traversing through a DIRC in Figure (1).

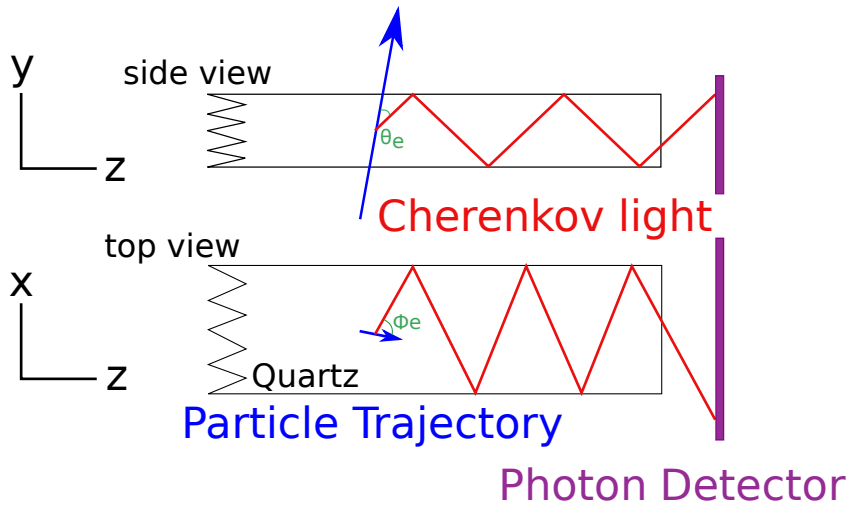

FIG. 1. Schematic diagram of a DIRC. Both panels display a particle penetrating the DIRC's quartz bar, and the path of the resultant radiation (Cherenkov light). Particles always penetrate the bottom wall (on the $xz-$plane) and travel inside releasing Cherenkov light at their Cherenkov angle θ_e determined by Eq. (1) with a polar angle ϕ_e uniformly distributed from 0 to 2π. This light travels to the photon detectors at the ends of the DIRC. The Cherenkov light's position, angle, and time is recorded here. (Note: each end along the z-axis has a photon detector.) The particle's trajectory is in blue, while the Cherenkov light's trajectory is in red. The top panel displays the side view (on the $yz-$plane) of this phenomenon, while the bottom panel displays the top view (on the $xz-$plane).

The DIRC at BaBar

A DIRC was first used in the BaBar detector at the Stanford Linear Accelerator Center (SLAC) to study the Charge Parity (CP) violation in the decays of B^0 mesons from Υ (4s) produced by the asymmetric e^+e^- collider PEP-II [3]. In order to study CP violation, high quality particle identification for kaons (K) and pions (π) was needed over a large range of solid angle and momentum [3]. Their PID algorithm was developed to perform well over the range of $700MeV/c$ to $4GeV/c$, allowing for π-K separation well above four standard deviations[3].

Their DIRC consisted of quartz bars of thickness 1.72cm, width 3.5cm, and length 490cm, with index of refraction $n = 1.474$ [3]. Light from all bars was detected by one photon detector with a resolution of 7mrad[3].

Our DIRC and PID algorithm

Particles typically seen in high-multiplicity events include Kaons (K), Pions (π), Electrons (e), and Protons (p). Of these particles, the most difficult separation is e-π separation. For this reason, we have focused on this separation at increasing levels of multiplicity.

As a reference we have modeled the DIRC after the DIRC used in the BaBar experiment [3]. We use its specifications in all Monte Carlo simulations and in all analyses. Instead of using one photon detector for all bars, we use 2 cameras per bar (one at each end of the bar along the $z-$direction).

METHODS

In order to model and test our DIRC and PID algorithm, we have created a Monte Carlo that generates particles and simulates their trajectory inside the DIRC. It outputs the photon information that one would obtain from a DIRC detector. Currently, we study one DIRC at ($R = 100$cm, $\eta_b = 0$) on the $y, x-$place (see Figure (2)).

The Monte Carlo is implemented through two libraries. The first (called the Particle-Generator) is used to generate particles and the second (called the Photon-Generator) to simulate particle(s) traversing through the DIRC and output the resultant photon information.

Once the photon information is produced, it is studied with a third library, the Particle-Reconstructor. We attempt to reconstruct the identity of each particle that entered the DIRC by studying the relation between the photon information and the particle's trajectories. We assume knowledge of the momentum and impact points of each particle.

All libraries for this project have been written in C++. For further analysis, a number of scripts have been written in C++ and Python. All scripts and libraries used for this project are agglomerated into the larger library, dirc-detector. It is hosted on GitHub[4]. This library relies extensively on the Data Analysis Framework ROOT [5].

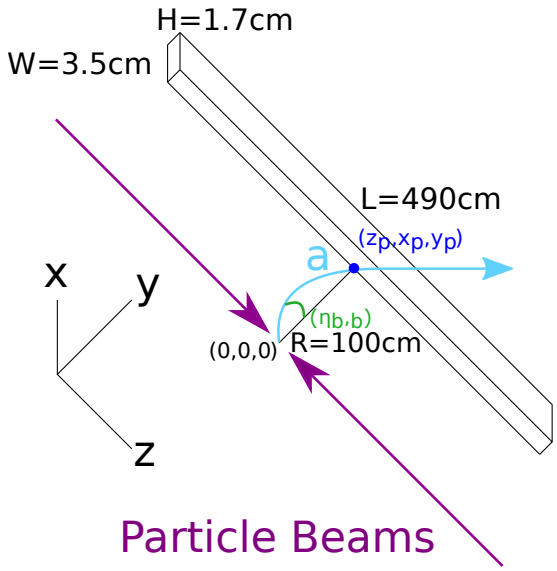

FIG. 2. This diagram is a visual representation of the particle generation process. All particle's are created with starting coordinates (0,0,0). A particle's initial direction is defined by angle (η_b, ϕ_b) (η_b is on the $yz-$plane with $\eta_b = 0$ being on the $y-$axis, and ϕ_b is on the $xz-$plane with $\phi_b = 0$ being on the $z-$axis). A magnetic field gives rise to a curvature in the particle's trajectory. This trajectory is labeled a (for arc) on the diagram. In our analysis, we have one DIRC situated at $\eta = 0$ at a distance of $R = 100$cm. Particles intersect this DIRC on the $xz-$plane at some (z_P, x_P, y_P). They are then further used in our Monte Carlo.

MONTE CARLO

Particle Generation

In this stage of the Monte Carlo, we generate particles that would be emitted from a beam collision. All particle are emitted from a single point $(z = 0, x = 0, y = 0)$. Timing for each particle begins when the particle is emitted. Particles are emitted with pseudorapidity η_b and azimuthal angle ϕ_b. Here, η_b has a uniform distribution about $(-.5, .5)$, while ϕ_b has a uniform distribution about $(0, 2\pi)$. Each particle has an equal probability of having a negative or positive charge. All particles are emitted with momenta probability that follows a steeply falling momentum distribution:

$$P(p) = A\frac{\frac{p}{GeV/c}}{\frac{1}{2} + (\frac{p}{GeV/c})^4} \tag{4}$$

where $P(p)$ is the probability of a particluar momentum value p, and A is a normalization constant. The domain of the momentum is confined to $(0 : 3)$GeV/c. $P(p)$ is normalized such that its integral over the range from $0GeV/c$ to $3GeV/c$ is 1. There are 4 choices for the particles that will be emitted:

Particle	Mass (GeV/c^2)
e	$.511 \times 10^{-3}$
π	0.140
K	0.494
p	0.938

each with an equal probability of being chosen.

Once a particle is emitted, its trajectory is calculated in order to determine whether it will intersect with the DIRC. Defining N_P as the number of particles emitted from the beam collision, N_P^{max} as the maximum number of particles to be emitted, N_i as the number of particles that intersect with the DIRC, and N_i^{dirc} as the desired number of particles to intersect with the DIRC– particles are emitted from the beam collision until either $N_i = N_i^{dirc}$ or $N_P = N_P^{max}$. $N_P = N_P^{max}$ only occurs when $N_i \leq N_i^{dirc}$. Once a particle is determined to intersect with the DIRC, its time of flight is calculated as

$$t_P = a/v_P \tag{5}$$

where a is the arc length from $(0, 0, 0)$ to the coordinate of intersection (z_P, x_P, y_P). The number of photons which it will produce per unit length in the DIRC (photons/cm) is determined by

$$\frac{dN}{dx} = 2\pi z^2 \alpha (1 - \frac{1}{n^2\beta^2}) \int_{200\times10^{-9}m}^{900\times10^{-9}m} \frac{d\lambda}{\lambda^2} \tag{6}$$

where λ is the wavelength range of interest and α is the fine-structure constant (approximately $7.297 \times 10^{-3} C^2/(eV \cdot F)$ [6]. We choose the a λ range of $(200 : 900) \times 10^{-9}m$ because that is the approximate wavelength transparency range for the material of our DIRC, quartz.

Photon Generation

At this stage, each particle's trajectory within the DIRC is simulated. The length of the path ρ within the DIRC that each particle will take is calculated. It depends on the impact point and angle. The expected number of photons that each particle will release is then determined by using (6) as $E_E = \rho\frac{dN}{dX}$. The actual number of photons to be produced by a particle follows a poisson distribution with mean E_E. Each photon is produced in the following manner:

1. A point between 0 and ρ along the particle's trajectory, ρ', is randomly chosen as the emission point.

2. The photon is emitted with angles θ_e, ϕ_e with respect to the particle's direction of travel where θ_e is determined by Eq. (1) and ϕ_e is randomly chosen between 0 and 2π.

3. The photon inherits its particle's time of flight to the DIRC t_P, along with the time necessary for that particle to travel to ρ_i as its starting time.

4. Each photon has a velocity $v = c/n$.

After being produced in the frame of the particle, each photon is rotated into the frame of the detector and its path in the DIRC is simulated as follows:

1. We seperate each photon velocity into 3 components (z, x, y) and find the photon's time of travel to each wall of the DIRC bar (w_z, w_x, w_y). The time to travel to each DIRC wall is calculated as $t_j = \frac{d_j}{v_j}$ where $j = z, x, y$, d_j is the distance to wall w_j, and v_j is the velocity along the $j-$axis. The wall corresponding to the lowest t_j is chosen–if two compete, one is randomly chosen among the two.

2. The angle with which the photon will reflect off a wall is determined by

$$\Theta = cos^{-1}\left(\frac{(\vec{v})\cdot(-\hat{n_j})}{|\vec{v}||\hat{n_j}|}\right),$$

where $\hat{n_j}$ is a unit vector along the $j-$axis. If $\Theta < \Theta_c$, where Θ_c is calculated with (3) as 0.745rad ($\sim \pi/4$), then the photon is eliminated from the list.

3. If the photon wasn't eliminated, it reflects and this process continues until the photon reaches one of the open ends of the DIRC bar.

4. Once the photons hit the detector surface, their final (θ, ϕ) is smeared by a gaussian distribution centered at 0 with a width equivalent to our single photon resolution of $1\sigma = 10$mrad. This resolution both handles the resolution of the photon detector and the deviations in angle caused by imperfect reflections.

This marks the end of the Monte Carlo.

PID

Single-Particle Analysis

The first step in this analysis was to study the response to one particle. We developed the following algorithm.

Each photon will most likely have reflected off a wall along the $x-$ and $y-$direction. We determine all possible photon angles by accounting for all possible reflections. This results in $(\theta, \phi) = (\pm\theta, \pm\phi)$, one of which corresponds to the original (θ_e, ϕ_e).

After determining all possible photon angles, we use the known trajectory of each particle to rotate each photon into the frame of each particle. All unphysical photon angles (e.g. all angles with $\theta > \frac{\pi}{2}$) are eliminated.

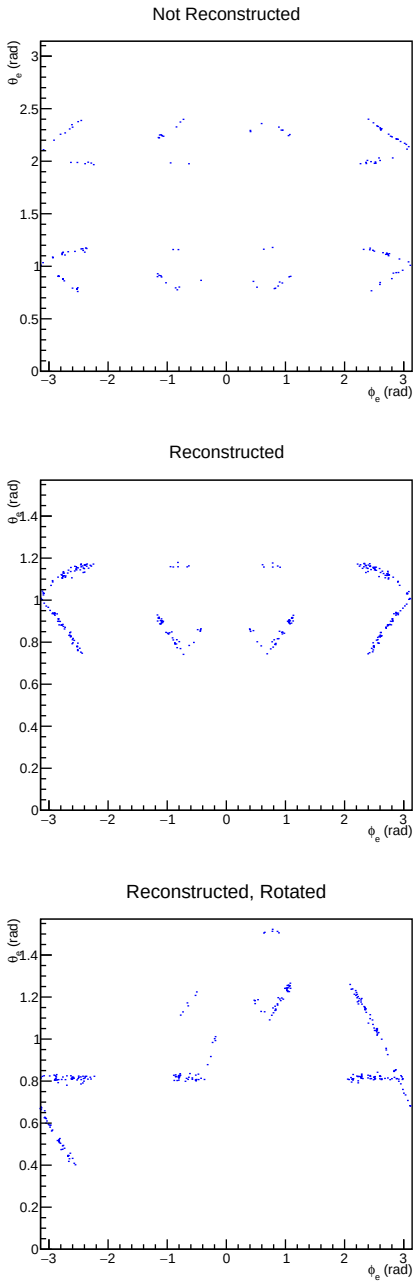

FIG. 3. **Top**: Distribution of all photon angles captured on the photon detector surface. **Middle**: Distribution of all possible photon angles $(\pm\theta, \pm\phi)$. **Bottom**: All the possible photon angles rotated into the frame of a particle trajectory.

This is done for each particle, seperately. For example, if there were a total of 2000 photons and 6 particles detected, all 2000 photons would be rotated in to the frame of each particle. An example of this process is shown in Figure (3).

Rotation into the particle's frame produces a concentration of photon angles at θ_e. This can be seen in the third plot in Figure (3), where the $\theta-$axis has a clear

straight line at $\theta \sim .8$. Thus, it can be used to statistically calculate θ_e for a particular particle. All analysis done on the photons in this rotated frame produces results for only that particle.

(As a reminder, E_E has been used as the expected number of emitted photons–E_F will be used as the found number of emitted photons. Following this convention, θ_E will refer to the expected θ_e value and θ_F to the found θ_e value.)

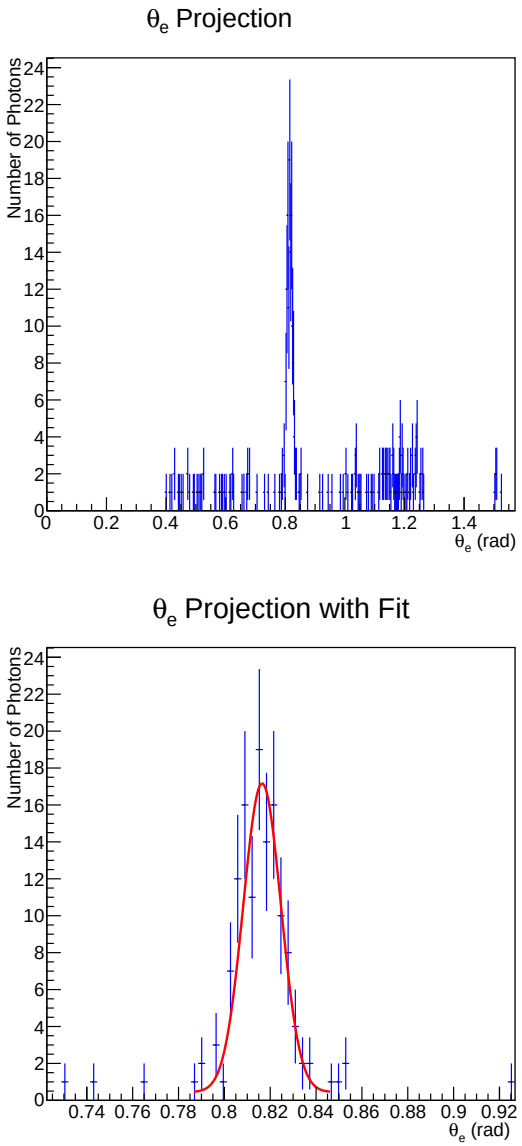

FIG. 4. **Top**: θ_e-projection of the photon angles rotated into the frame of a particle. The rotated photon angles are those in the bottom panel of Figure (3). **Bottom**: A zoomed-in plot of the plot above with Eq. (7) fit. The fit does not extend beyond a few sigma away from the gaussian center, so as to ensure that most angles used are correct photon angles.

In order to statistically calculate a particle's θ_e, we apply a fit to the θ_e-projection of rotated photon angles. In Figure (4), we show the θ_e-projection of the rotated photons displayed in the the bottom panel of Figure (3). In the bottom panel of Figure (4), we see that the photon angle distribution resembles a gaussian distribution, thus a gaussian distribution is fit.

By considering every photon reflection in our analysis, we both increases our background noise and the number of correct photon angles used in our gaussian fit. We account for this background noise by fitting a gaussian distribution plus a constant

$$f(\theta) = ae^{\left(-\frac{(\theta-\theta_F)^2}{2\sigma_\theta^2}\right)} + b \tag{7}$$

where θ_F takes on the emission angle of the different particle types, σ_θ the single photon resolution (1σ), a is the gaussian amplitude, b the gaussian center, c the gaussian width, and d a constant accounting for the background.

Because we are dealing with the separation of a finite set of particles (K, π, p, e), we know θ_e can only be one of 4 values. As we know the momentum of the particle and each particle type has an associated mass, for every possible particle type, we can use Eq. (1) and Eq. (2) to determine the expected emission angle θ_E.

As long as we fit the gaussian locally (as is visible in the bottom panel of Figure (4)), we primarily fit the correct photon angles, thus primarily benefitting from using all possible photon angles $(\pm\theta, \pm\phi)$. Using gaussian statistics, we can capitalize on the fact that the accuracy of obtaining the particle's θ_e via a gaussian fit increases in proportion to the square-root of the gaussian's integral E_F (our resolution increases from 1σ to $1\sigma/\sqrt{E_F}$).

We also use Eq. (7) to determine the number of photons emitted by a particle. We calculate the integral (which includes the spread of θ_e values by a smearing of 1σ) to be E_F:

$$E_F = \int_{-\infty}^{\infty} (f(\theta) - b)d\theta. \tag{8}$$

Single-Particle Performance

The accuracy of θ_F is directly dependant on the number of photons detected E_F. Thus, we use a resolution of $\sigma_d = 1\sigma/\sqrt{E_F}$.

The deviation from the expected value $\theta_F - \theta_E$ is quantified in terms of the resolution σ_d as

$$\Delta\sigma_\theta = \frac{(\theta_F - \theta_E)\sqrt{E_F}}{1\sigma} = \frac{(\theta_F - \theta_E)}{\sigma_d}. \tag{9}$$

Similarly for $E_F - E_E$, the deviation is quantified as

$$\Delta\sigma_E = \frac{(E_F - E_E)}{\sqrt{E_E}}, \tag{10}$$

E_E depends on a particle's type. We calculate it as follows:

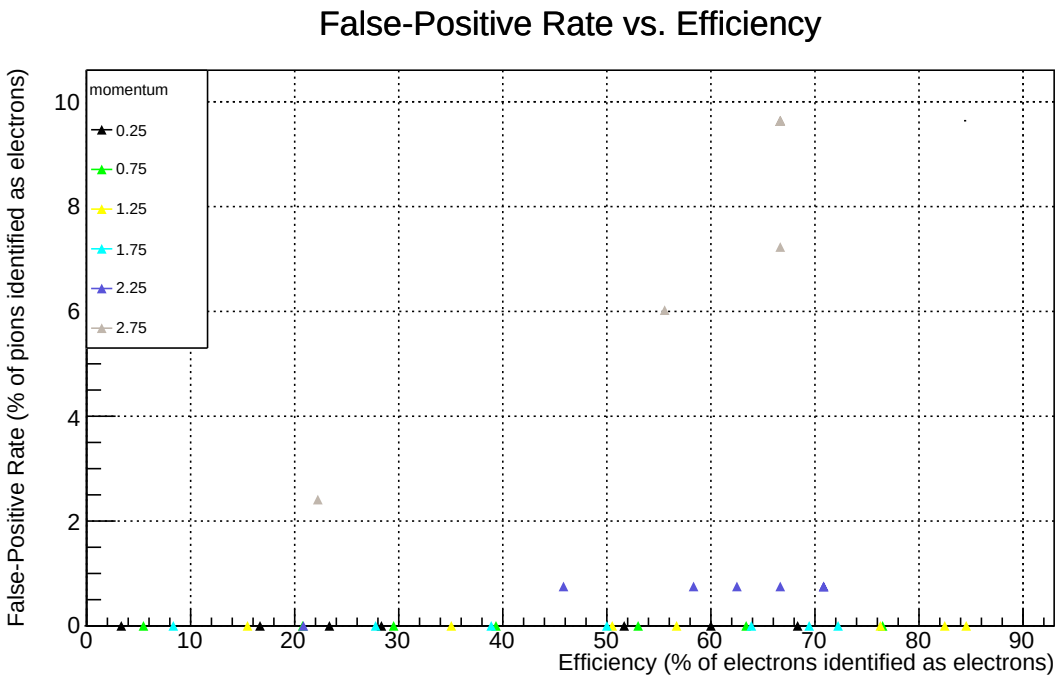

FIG. 5. Plot of f vs. e for single-particle events. Events with pions were used for f, and events with electrons were used for e. Each momentum value encompasses all values within $.25GeV/c$, e.g. $p = 2.25$ corresponds to $p = (2 : 2.5)GeV/c$. f remains at $\sim 0\%$ with e as high as 90% until $p = 1.75$. f rises to $\sim 1\%$ with maximum $e \sim 70\%$ at $p = 2.25$, afterwards it rises to just below 10% with maximum e lowering to just $\sim 65\%$ at $p = 2.75$. We see that the f vs e begins to show an appreciable increase at $p \sim 2.75$.

For a particular particle and assumed particle type, we emit 50 photons with θ_e corresponding to that particle and ϕ_e evenly distributed around $(0 : 2\pi)$ at 100 discrete steps along that particle's path length. The total number of photons released is T. A photon requires an angle greater than Θ_C (approximately $\pi/4$) with respect to the wall its reflecting off in order to pass the critical angle cut. Reflecting with such an angle, after each reflection, a photon should travel to an adjacent wall. We allow photons to reflect 3 times. After 3 reflections, one of the z, x, and y walls should have been reflected by the photon. As the angle with which a photon will reflect off a wall is consistent due to snell's law, after 3 reflections, it should be apparent whether a photon will or will not pass the critical angle cut. If a photon passes the critical angle cut it contributes to P. E_E is then calculated as

$$E_E = \rho \frac{P}{T} \frac{dN}{dx}$$

where ρ is the particle's path length and $\frac{dN}{dx}$ corresponds to (6), the number of photons per unit length.

Despite the critical angle cut, we treat to E_E to be a poisson statistic, thus using $\sqrt{E_E}$.

A particle is identified as a certain type if the uncertainty for that type is below some threshold m, i.e., $\Delta\sigma_E$ and $\Delta\sigma_\theta$ are both below m:

$$|\Delta\sigma_E| < m, \tag{11}$$

and

$$|\Delta\sigma_\theta| < m. \tag{12}$$

Every particle has a $|\Delta\sigma_i|$ (where $i = E, \theta$) for each of the 4 possible particle types, π, p, e, K. If multiple particle types have a $|\Delta\sigma_i| < m$, the particle type with the smallest $|\Delta\sigma_i|$ is chosen as the particle's identity. Suppose there is an pion with the following:

Particle Type	$\lvert\Delta\sigma_i\rvert$
π	.8
e	.5
K	12
p	4.2

If $m \geq .5$, the pion will be identified as an electron, if $m < .5$, we conclude that the analysis was unable to resolve the particle's identity.

In order to analyze our PID algorithm, we study the percent with which we false-positively identify a particle by another type and the percent with which we correctly

identify a particle as itself. We call the former our false-positive rate f and the latter our efficiency e. For example, our false-positive rate could be defined by the proportion of instances in which a electron was false-positively identified by a pion, whereas the efficiency could be the proportion of instances in which an electron was correctly identified by an electron. We study the evolution of f in terms of e by varying m. As m increases, it is easier to identify a particle as itself but it also becomes easier to identify a particle as another particle.

Returning to the example above, studying the false-positive rate of electrons as pions, we would vary the threshold and see how often a pion is identified as either a pion or electron. The example particle would have contributed to f if $m \geq .5$.

As e-π seperation is the hardest seperation we face, this is how we tested our algorithm in for single-particle events. One can see our f vs. e plot in Figure (5). We were able to retain high discrimination ($f < 1\%$) until $p = 2.5GeV$. At higher momentum, we maintained $f < 10\%$.

The $\Delta\sigma_i$ distributions produced neither have a width of 1 corresponding to $1\sigma_i$, nor are they centered at 0. This makes it more cumbersome to determine the m value(s) to cut $\Delta\sigma_i$ on. To faciltiate this process, we calibrate all $\Delta\sigma_i$ values. This calibration process centers all $\Delta\sigma_i$ distributions at 0, and casts σ_i as the the width of the distribution. By doing so, all decisions of whether a particle will or will not be identified as a particle type is simplified to determining if $|\Delta\sigma_i| < m$, rather than calculating specific m values per distribution. We avoid one more complication: as $\Delta\sigma_i$ is dependent on θ_e which is dependent on momentum, $\Delta\sigma_i$ is indirectly related to momentum. This requires that we determine m values for specific momentum ranges for each distribution. We avoid this. Details on this calibration can be found in the appendix.

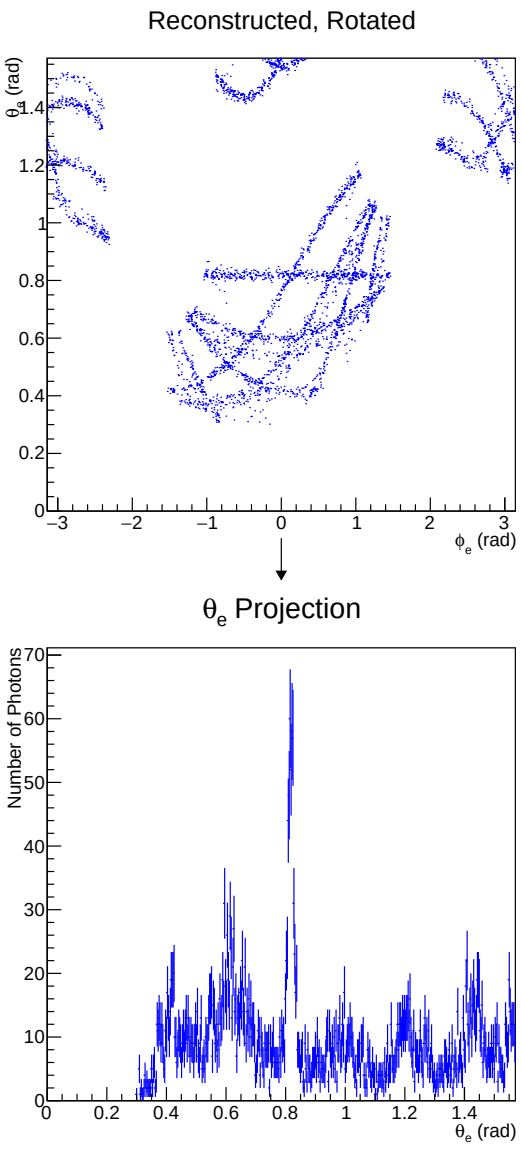

FIG. 6. **Top**: A distribution of photon angles from multiple particles rotated into one particle's frame. While the background is larger than with 1 particle, it is easy to visually recognize the particle's emission angle ($\sim .8$). **Bottom**: The theta projection of the distribution. A peak at $\sim .8$ corresponding to the emission angle clearly sits atop a large and variable background.

Multi-Particle Analysis

As the number of particles that enter the bar increases, for a particular particle, θ_F may shift away from θ_e due to the large number of cherenkov photons not associated with the particle being investigated.

In Figure (6), one can clearly see the non-linear background that surrounds the peak at θ_e. While a gaussian plus constant provides a decent fit to Figure (6), the accuracy σ_d is compromised and misindentification becomes more likely. The background makes it unclear which photons belong to the particle and which do not. When fitting Eq. (7), d can easily take a value that is too large or too small. This makes E_F innacurate. This is especially true for cases, such as the one in the second plot of Figure (6), where the background is not constant. In summary, both θ_F and E_F can show appreciable deviation from their true values.

In order to mediate this problem, we index the photons by the particle we posit that they belong to. Looking at Figure (6), one can still see clear peaks in the vicinity of the θ values which correspond to the particle's emission angle. This observation is used to index the photons.

We first rotate all photons into the frame of a particular particle. In the particle's frame, we search for the peak θ in the general vicinity of θ_E (within 5σ) and label it θ'_e. Once θ'_e is found, we associate all photons with

$|\theta'_e - \theta_e| \leq 3\sigma$ to that particle. Every index corresponds to a particle–if a photon has a θ_e within 3σ of θ'_e for multiple particles, it is marked as ambiguous. In Figure(7), we have color coded the photons associated with individual particles. All photons that are marked as ambiguous are colored black.

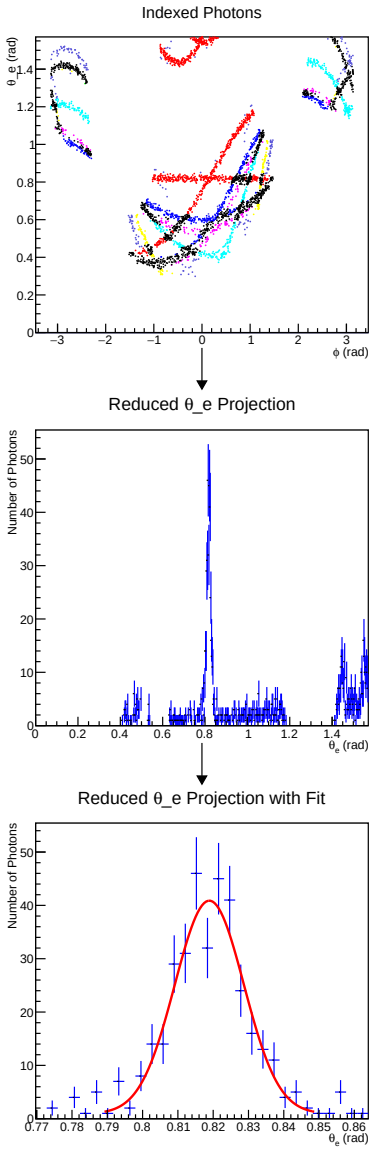

FIG. 7. **Top**: The distribution in the top panel of Figure (6) with each photon colored by its particle membership. Photons of ambiguous membership are colored black. **Middle**: The θ_e-projection of the photons associated to the red particle. There is a clear improvement in the level of background. **Bottom**: Gaussian fit to the θ_e-projection above.

After all photons have been indexed, each particle and its associated radiation is analyzed. Just as before, we fit (7) to the $\theta-$projection of the photons in the particle's frame. However, this time, we only create a projection of the θ values for photons associated unambiguously with the particle of interest. In the case of Figure (7), only photons colored red were used in the middle plot. Photon sets with sufficiently low counts (< 50) are discarded as un-analyzable.

RESULTS

For all results, f_i was defined as the number of times a pion was identified as an electron in a particular momentum range Δp_i and e_i the number of times an electron was identified as an electron in a particular Δp_i. Particle generation is restricted to the generation of pions or electrons as e-π separation is the most difficult separation we face.

Low-Multiplicity: $N_P^{dirc} = 1$

For this study, we separately generated 3000 events of either strictly pions or strictly electrons with $N_P^{dirc} = 1$. We found our f_i to remain below 5% with e_i up to 90% for $p < 2.5GeV/c$. At momentum higher than 2.5GeV/c, f remains below 10%.

Medium-Multiplicity: $N_P^{dirc} = 6$

For this study, we first generated 2000 events of strictly pions with $N_P^{dirc} = 5$. In order to study f_i we embedded one pion with p following the distribution defined by (4); for e_i the same procedure was involved except electrons were embedded in place of pions. We found our f_i to remain below 5% with e_i up to 60% for $p < 2GeV/c$.

CONCLUSION

We have developed a PID algorithm capable of disentangling radiation information for strong particle separation with a minimal f_i for $p < 2GeV/c$. This PID algorithm has not yet utilized the temporal distribution of the particle's radiation, something we believe will be a key factor in pushing our success to higher multiplicities.

Calibration

Data calibration consists of two steps: (1) generating a calibration distribution and (2) applying the calibration distribution to a data set. Step (1) is only performed once per major change to the Monte Carlo and ParticleReconstructor, while step (2) is applied to every data set of particle reconstructions.

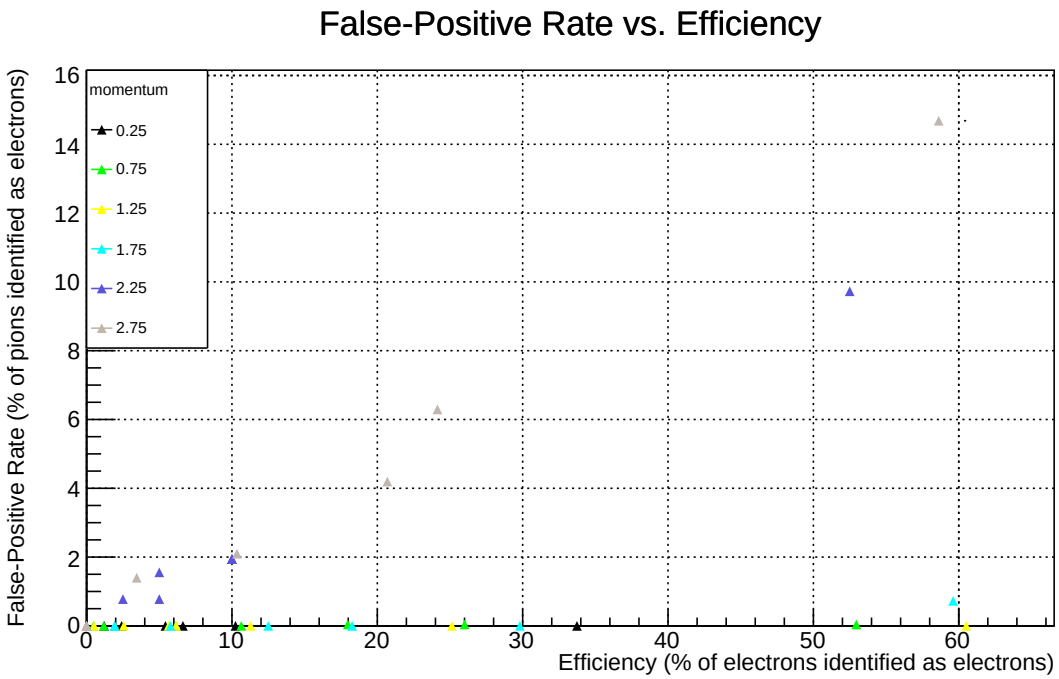

FIG. 8. Plot of f vs. e for 6-particle events. All events had 5 pions. A pion was embedded for f, and an electron for e. f remains at $\sim 0\%$ with e as high as 60% until $p = 1.75$. f rises to as high as $\sim 10\%$ with maximum $e \sim 50\%$ at $p = 2.25$. It then rises to just $\sim 15\%$ with maximum $e \sim 65\%$ at $p = 2.75$. We see that the f vs e begins to show an appreciable increase at $p \sim 2.25$ rather than $p \sim 2.75$ like with single-particle events.

Calibration distributions are generated per particle type. In order to generate the distribution for a particular type, a monte carlo is run with 10,000 events, each containing one particle of the desired type. The Particle Reconstructor generates a distribution of σ_θ and σ_E values. These values are sorted by the *momentum* of the associated particle. σ_θ and σ_E distributions are separated into clusters by momentum ranges of $\Delta p = .25 GeV/c$. For each distribution, a gaussian $g(x)$ is defined whose center C is nearby the distribution peak and whose width W is defined as the domain about C which produces an integral $G(x)$ such that

$$G(x) = \int_{C-W}^{C+W} g(x)dx \sim .68\% \int_{C-5W}^{C+5W} g(x)dx$$

of the counts of the distribution.

Each particle reconstruction is calibrated via

$$\sigma_i = \frac{(\sigma_i - C_i)}{W_i},$$

where $i = \theta, E$. Separate calibration distributions are produced for both the radiation and the emission angle uncertainties.

We would like to thank the NSF, DOE, and SUNY research foundation for funding this research project.

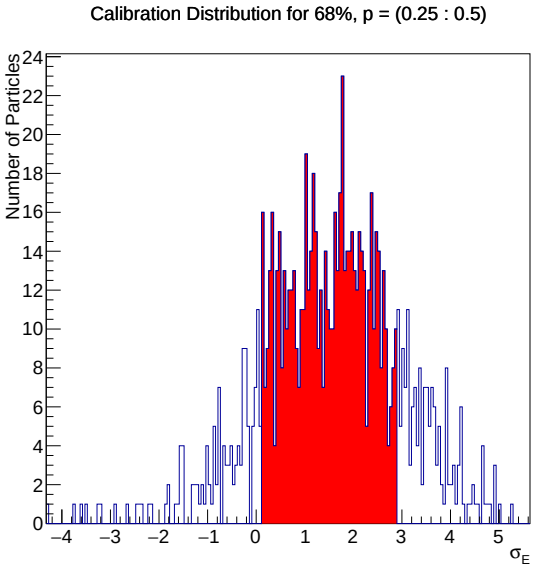

FIG. 9. A sample $\Delta\sigma_E$ distribution. It is centered at ~ 1.4 with width ~ 1.1. It was centered at 0 and adjusted to have width 1 corresponding to the region shaded red.

* wilka.carvalho@stonybrook.edu

[1] J. Séguinot and T. Ypsilantis, Nuclear Instruments and Methods in Physics (1999).
[2] I. e. a. Adam, Nuclear Instruments and Methods in Physics **538**, 281 (2005).
[3] I. Adam, R. Aleksan, D. Aston, P. Bailly, C. Beigbeder, M. Benayoun, M. Benkebil, G. Bonneaud, D. Breton, H. Briand, *et al.*, Nuclear Instruments and Methods in Physics Research Section A: Accelerators, Spectrometers, Detectors and Associated Equipment **433**, 121 (1999).
[4] Https://github.com/wcarvalho/dirc-detector.
[5] R. Brun and F. Rademakers, Nuclear Instruments and Methods in Physics Research Section A: Accelerators, Spectrometers, Detectors and Associated Equipment **389**, 81 (1997).
[6] K. Olive *et al.* (Particle Data Group), Chin.Phys. **C38**, 090001 (2014).